Impact of drying on meso- and nano-scale structures of citrus fiber: A study by SFG, ATR-IR, XRD, and DLS

Mohamadamin Makarem[1], Hyojung Kim[1], Parinaz Emami[1], Jesus Melendez[1], Adam Steinbach[2], Tristan Lipkie[2], Isabelle Deleris[3], Christina Desmet[3], Jöel Wallecan[3], and Seong H. Kim[1*]

[1]Department of Chemical Engineering, Materials Research Institute, Pennsylvania State University, University Park, Pennsylvania 16802, United States
[2]Cargill Research and Development, Plymouth, Minnesota, 55447, United States
[3]Cargill Research and Development, 1800 Vilvoorde, Belgium

* Corresponding author: shk10@psu.edu

Abstract

Citrus fibers are a byproduct of the pectin extraction process from citrus peel. This by-product can be converted into a functional ingredient through a shear-induced homogenization process. One technical challenge with this material is that dehydration and subsequent rehydration results in reduction of viscosity compared to the original product. In this study, various drying methods were compared with never-dried fibers to investigate the structural changes underlying the viscosity loss. Infrared and x-ray diffraction analyses confirmed no changes in chemical composition and crystalline structure of citrus fibers. The dynamic light scattering and sum frequency generation analyses of citrus fiber suspension showed that the rehydration process could not fully disperse aggregated fiber, which appears to be the main cause for the viscosity loss.

25 TOC

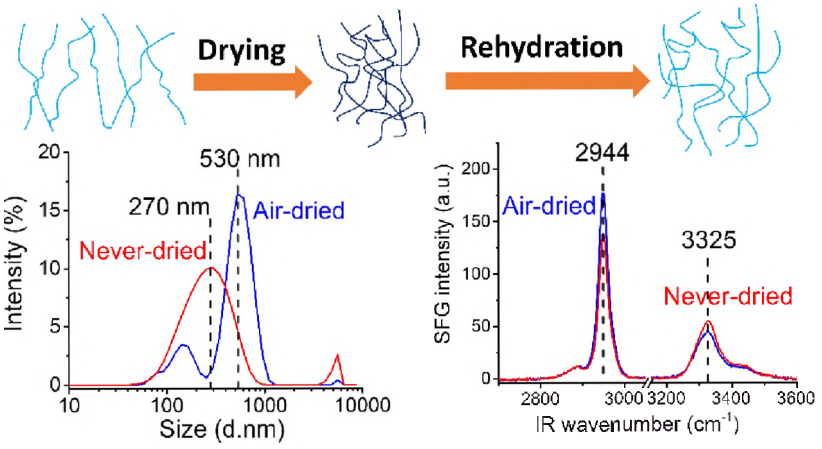
Drying
Rehydration
530 nm
270 nm
Air-dried
Never-dried
Intensity (%)
Size (d.nm)
2944
Air-dried
3325
Never-dried
SFG intensity (a.u.)
IR wavenumber (cm-1)

26

Introduction

Food, pharmaceutical, textile, and paper are among major industries utilizing plant cell walls. During the processing of agricultural products, there can be a vast amount of plant-based byproducts with low value. Finding solutions to turn these byproducts into desirable goods can help industries to step toward a complete usage of raw materials. This study focuses on the structure of spent citrus peel, the residual material after pectin extraction. Citrus peel can be valorized into functional fibers by high shear processes, such as homogenization. Citrus fibers can be used as functional ingredients in the food industry to improve viscosity, water binding, emulsification amongst other properties.[1-2]

The viscosity of fiber suspensions plays a crucial role in producing a food ingredient with desirable texture and quality. Citrus fibers are first functionalized by high shear processing to create a viscous suspension. The citrus fibers are mainly consisted of primary cell walls with less than a micron in thickness, thus the high shear processing can break these walls into smaller fragments and expose cellulose fibers. Then, fibers are dried for storage and distributed as a food ingredient. In use, they are rehydrated and mixed with other food ingredients. Rehydration of dried fibers typically results in a viscosity lower than the product before dehydration. This is thought to be due to the structural changes in fibers during the dehydration process.[3-4] In order to find ways to improve the viscosity of rehydrated suspensions, the cause of viscosity loss during dehydration should be better understood. Answering such questions requires a comprehensive understanding of the chemical and physical properties of the citrus fibers before, during, and after drying.

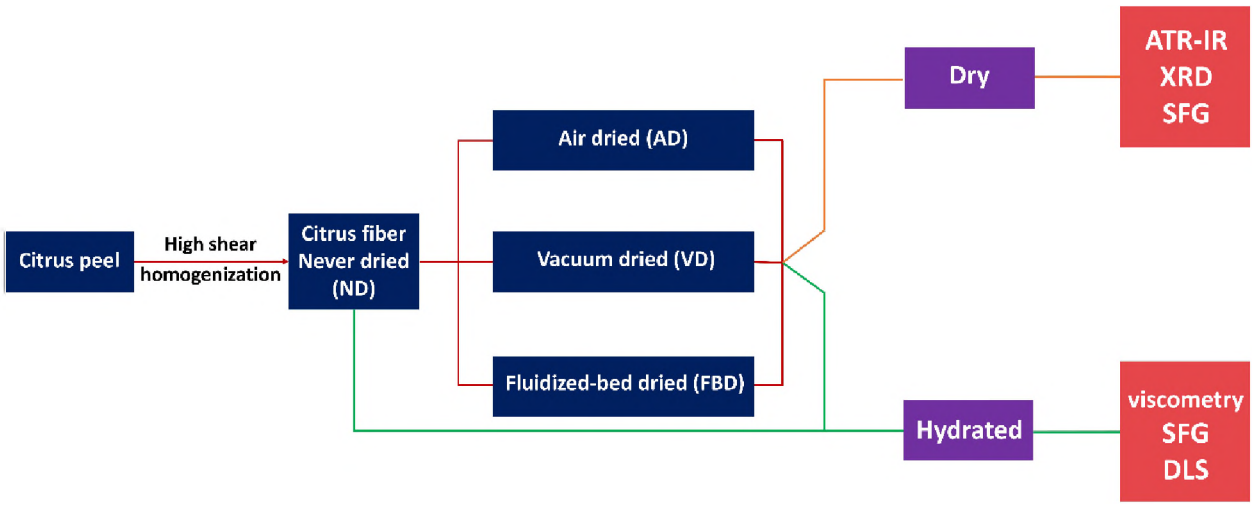

Scheme 1. The experimental procedure applied in this study to understand the impact of dehydration on nano- and meso-scale structure of citrus fibers

In this study, the structural changes associated with viscosity loss in rehydrated citrus fibers were investigated using an approach (Scheme 1) combining infrared (IR) spectroscopy, x-ray diffraction (XRD), sum frequency generation (SFG) vibrational spectroscopy, and dynamic light scatterning (DLS) which is demonstrated in Scheme 1. The pectin depleted citrus fiber used in this study is an amalgamate of cellulose microfibrils, pectin, and hemicellulose. Cellulose content is typically more than 50% of the dry mass. IR was used to monitor compositional changes in the dried citrus fiber. XRD was used to check any differences in crystalline structure of cellulose in fibers dried in different methods. DLS was used to analyze the particle size distribution of citrus fibers in the hydrated state. SFG was used to investigate meso-scale structural features of cellulose interspersed an amorphous matrix[5-7]. Cellulose is SFG-active because of its noncentrosymmetric crystal structure. Other cell wall polymers, such as pectin and hemicellulose, form an amorphous matrix in a hydrated state, which makes them SFG-inactive[6, 8]. SFG is sensitive to the cellulose crystal structure over a wide length scale,[9] including cellulose polymorphism[7], crystal

orientation[10], bundling of crystals[11], distance between crystals[12], and change in polar ordering of crystals[13]. The information obtained from all characterization techniques in this study proved that the change in viscosity due to drying originates from variation in mesoscale structure of cellulose fibers.

Experimental Methods

Citrus Fiber Sample Preparation

Citrus peel fibers were prepared at a pilot scale by Cargill R&D. "Spent peels" (i.e. lemon peel after acidic pectin extraction) (~12% dry substance) were diluted to 2.5% dry substance with reverse-osmosis (RO) filtered water and sieved through 1.0 and 0.5 mm sieves. Composition of lemon peel after acid extraction was prereviously reported[2] to be 28% pectin with 60% degree of methylation. Monosaccharide composition (mmol/g dry matter) was 0.39 galacturonic acid, 0.015 fucose, 0.036 rhamnose, 0.089 arabinose, 0.196 galactose, 0.038 glucose, 0.111 xylose, 0.025 mannose.

Samples were bleached to remove natural pigments in the citrus peel that can generate non-resonance interference in SFG analysis. The fiber was dispersed by homogenization with an Ultra-turrax mixer for 10 min at 8000 rpm. The fiber was precipitated with isopropanol (IPA), and an aliquot was collected as the "never-dried" (ND) sample. Fiber samples (200 g each) were dehydrated by either air drying (AD) at room temp (21 °C) for 72 hours, by vacuum drying (VD) at 60 °C and 250 mbar, or by using a STREA-1 fluidized bed dryer (FBD) from GEA (Kirchberg, Switzerland) with inlet air at 60°C and a representative sample for each drying technique was used for this study. Pellets were made from dried fibers using a hand-press pellet maker for ATR-IR, XRD, and SFG analysis.

87 *Viscosity of rehydrated citrus peel fiber suspension*

88 For dried fibers (>90% d.s., including AD, VD, FBD), 2wt.% solutions were made by
89 mixing 0.5 g of citrus fibers with 24.5 g of either DI water or D_2O. For ND, which was partially
90 hydrated (15% d.s.), the ratio of ND to water or D_2O (99.9%) was 3 g of ND to 22 g of DI water
91 or D_2O to make 2% d.s. suspensions. Hydration by D_2O instead of H_2O was required for SFG
92 measurements of fibers in the hydrated state because H_2O attenuates IR in the OH stretch vibration
93 region of cellulose. Each sample was hydrated by magnetic stirring overnight.

94 The viscosities of the hydrated samples were measured using an RM180 rotational
95 viscometer with a cylindrical measurement system. Measuring bob 1 (30 mm diameter) and tube
96 1 (32.54 mm) were used for every sample except ND. For the ND, due to its high viscosity,
97 measuring bob 3 (14 mm) and tube 3 (15.18 mm) were used. The shear rates ranged from $10s^{-1}$
98 to $100s^{-1}$ with steps every 10 s^{-1} at about 21.5°C.

99 *Analysis of citrus peel fibers*

100 FT-IR was measured using attenuated total reflectance infrared spectrometry (ATR-IR).
101 For ATR-IR citrus fibers were made into pellets. All ATR measurements were done using a Bruker
102 Vertex 70 spectrometer, at 5 cm^{-1} resolution and 2.6 cm/s optical velocity. XRD measurements
103 were done using a Xeuss 2.0 x-ray diffractometer with Cu tube (λ=1.5405A). The experiment were
104 done in transmission mode, the scattering angle from 5° to 42° was measured at the step size of
105 0.05° with 5-sec exposure at each step.

106 A broadband SFG system equipped with an 85 fs Ti-Sapphire amplifier system with a
107 2KHz repetition rate was used in this study. Laser system produces 800 nm and broadband IR
108 pulses. The SFG experiments were done in two geometries: reflection, and transmission. The

reflection geometry was used for analyzing fibers formed into pellets with a laser incident angle of 45° normal to the sample stage for both 800 nm and IR beam. SFG transmission was done for fiber suspensions prepared by D_2O. For SFG measurements were done in *ssp* polarization combination, the three-letter combination represents the polarization of SFG, 800 nm pulse, and IR pulse, respectively.

The distribution of hydrodynamic diameter of citrus fibers in suspensions was analyzed using a dynamic light scattering (DLS) system (Malvern Zetasizer NanoZS90). DLS measures the size of regions that have refractive index different from the medium through autocorrelation of scattered light intensity fluctuation. The average particle size obtained from DLS was close to hydrodynamic diameter[14]. The 2 wt.% solutions were diluted 10 times to reduce the concentration of particles in solution and then filtered using 8 μm mesh PVDF membrane from Millipore to reduce polydispersity of samples. The particles above 8 μm were filtered out so that the change in the size distribution of particles smaller than 8 μm could be monitored without interference from larger particles.

Results and Discussion

Decrease in viscosity of rehydrated suspension compared to the ND suspension

The shear rate dependent viscosities of fibers in a rehydrated state (AD, VD, FBD & ND) were measured in Figure 1. The viscosity profile is consistent with power-law behavior as evident with a linear response on a log-log scaling. The viscosity of ND suspension was higher in all shear rates compared to the rehydrated fiber suspensions. Among the rehydrated samples used in this

study, the lowest viscosity was observed with the FBD fiber. However, previous internal experiments conducted by Cargill suggested higher viscosities of FBD compared to other drying methods. Note that the viscosity of FBD suspension was highly dependent on its preparation procedure; by changing drying process parameters, the viscosity can increase and get close to AD and VD as shown in Figure S1. The AD and VD suspension had intermediate values between the ND and FBD values. The rehydrated samples had viscosities lower than the ND suspension regardless of the drying method. This implies that the fiber drying caused some irreversible (at least, not easily reversible) changes in physical or chemical structures of fibers. From this observation, the main focus of this study was to investigate the physical and/or chemical changes of citrus fibers upon drying that can be correlated with the loss of viscosity upon rehydration.

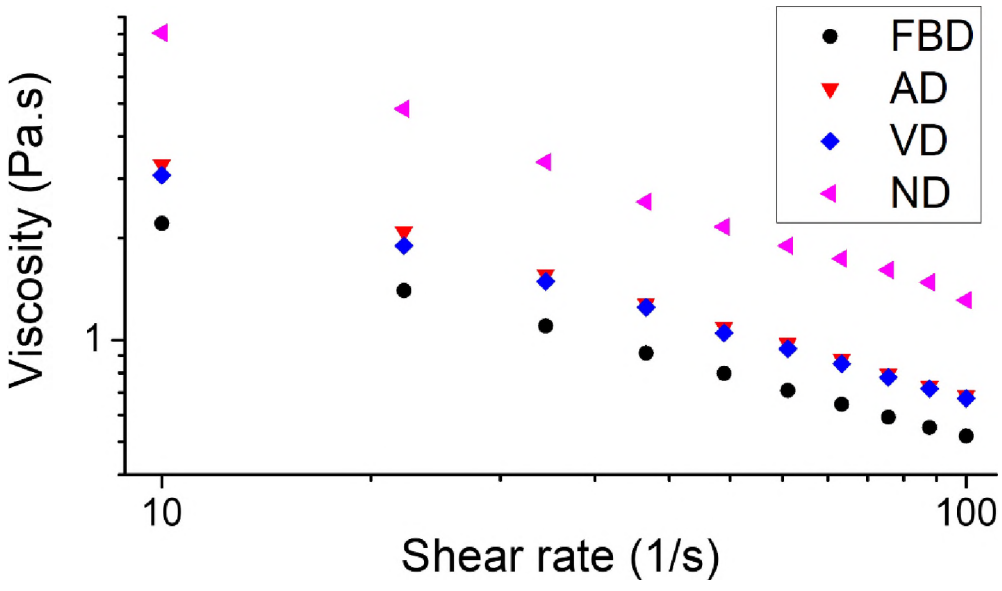

Figure 1. Viscosity of citrus peel fiber suspensions (2 wt.%) measured at various shear rates from 10 s^{-1} to 100 s^{-1}.

No discernable differences in chemical composition and crystallinity

ATR-IR spectroscopy was used to check chemical changes induced by drying. Cellulose, hemicellulose, and pectin all have very strong and complicated absorption bands between 850 cm^{-1} and 1200 cm^{-1} [15-17]. So, it is practically impossible to differentiate and assign the bands in this region to individual components[9, 18]. The peak at 1160 cm^{-1} is often attributed to the glycosidic C-O stretch of crystalline cellulose; but in the presence of hemicellulose and pectin, such assignment is not appropriate because the glycosidic C-O bonds of hemicellulose and pectin also show peaks close to that region.[9] The crystalline cellulose Iβ has a characteristic peak at 710 cm^{-1}, but its intensity is usually weak[19-21]. The peak at 1740 cm^{-1} is the C=O stretch mode characteristic of pectin[22-23]. Overall, the spectra shown in Figure 2(a) were very similar. This indicated that the drying methods had no impact on chemical composition of the citrus fiber. As expected, all components present in the ND sample were preserved in the dried sample.

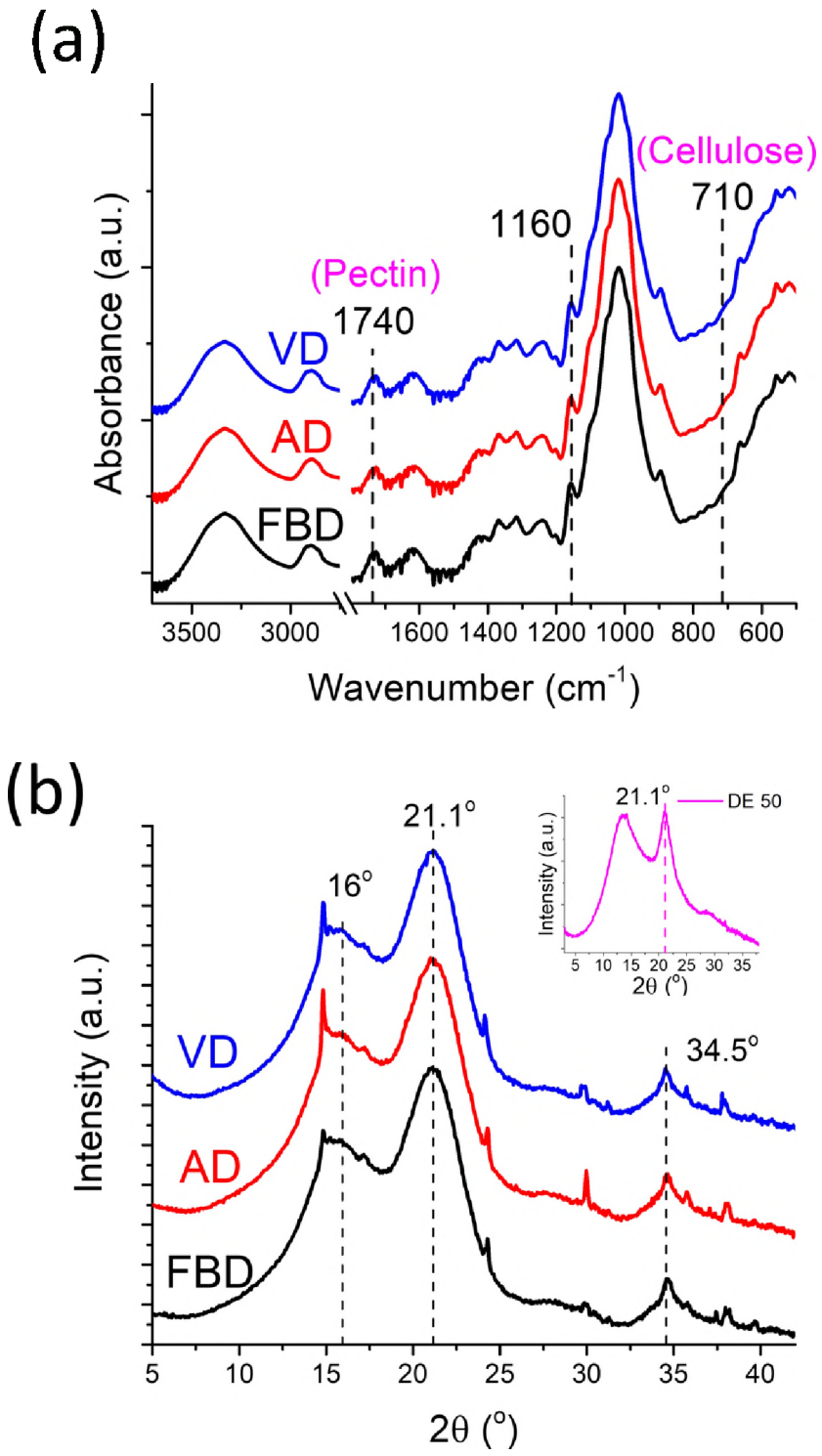

158

159 **Figure 2.** (a) IR spectra and (b) x-ray diffractorgrams of dried fibers. In (b), sharp small peaks are due to
160 salt particles in the sample. The inset to (b) shows the XRD data of pectin isolated from citrus peels prepared
161 by Cargill Inc.
162

Changes in the crystallinity of citrus fiber as a result of drying were investigated using XRD. The diffractograms of AD, VD, and FBD samples are compared in Figure 2(b). All samples exhibited two broad peaks at 2θ of ~16° and 21.1°, and a relatively sharp peat at 34.5°. Typical XRD data of cellulose Iβ have a large peak at 22.6° and two smaller peaks at 14.7° and 16.5°.[24-25] For the dried pectin, as shown in the inset of Figure 2(b), there are an extremely broad peak at 13° and a relatively sharp peak at ~21°. Thus, the broad peak at 21.1° in the diffractograms of AD, VD, and FBD samples must be the overlap of diffraction peaks from the residual pectin and cellulose in the citrus peel fibers. The 2 0 0 diffraction peak of cellulose at 22.6° cannot be clearly distinguished from the overlapped broad peak. The diffraction peak at 34.5° is the 0 0 4 diffraction peak of crystalline cellulose. The sharp diffraction peaks observed in figure 2, can be assigned to inorganic crystals in the citrus fiber samples. From the position of these diffraction peaks, it is possible to originate them to crystalline calcium oxalate,[26] which grows and remains incide plant cells and may remain in citrus fibers after processing of citrus peels.

The relative intensity and shape of main peaks at ~16°, ~21°, and 34.5° in figure 2 remained almost identical in the diffractograms of the AD, VD, and FBD samples. Thus, it can be said the crystallinity of cellulose did not vary noticeably with the drying method however the crystallinity and polymorphism could not be quantified from the broad measured diffractogram. So the variation in viscosity of different drying methods was not related to the change crystallinity of citrus fibers. The unchanged chemical composition and crystalline structure observed by IR, and XRD, led to the conclusion that drying did not affect the nanoscale structure; therefore, the change in mesoscale structure needed to be investigated.

Changes in size distribution of fiber aggregates in aqueous suspension

The IR and XRD analysis results of the AD, VD, and FBD samples (Figure 2) did not show any difference that can be correlated with the reduction of viscosity upon rehydration of those samples compared to the ND suspension (Figure 1). Then, the rehydrated properties needed to be examined. We analyzed the particle size distribution of the rehydrated fibers and ND using DLS. The resulting particle size distrubtions were found to be very broad presumably due to the original manufacturing process utilizing intensified mechanical shear forces. Previous studies on citrus fibers found no direct correlation between the size distribution of larger particles >10 μm and the viscosity of fibers.[2] It is expected that in samples with similar volume fraction of particles, if the colloidal particles have smaller hydrodynamic diameters they would have larger effective volume which results in higher viscosities.[27-28] Thus smaller particles would have large impacts on viscosity of the suspension with hydrated fibers. For this reason, we diluted 2 wt.% suspension solution to 0.2 wt.% and then filtered with an 8-micron cut-off PVDF membrane. Figure 3 shows the particle size distribution of AD, VD, FBD, and ND suspensions in the filtered solutions.

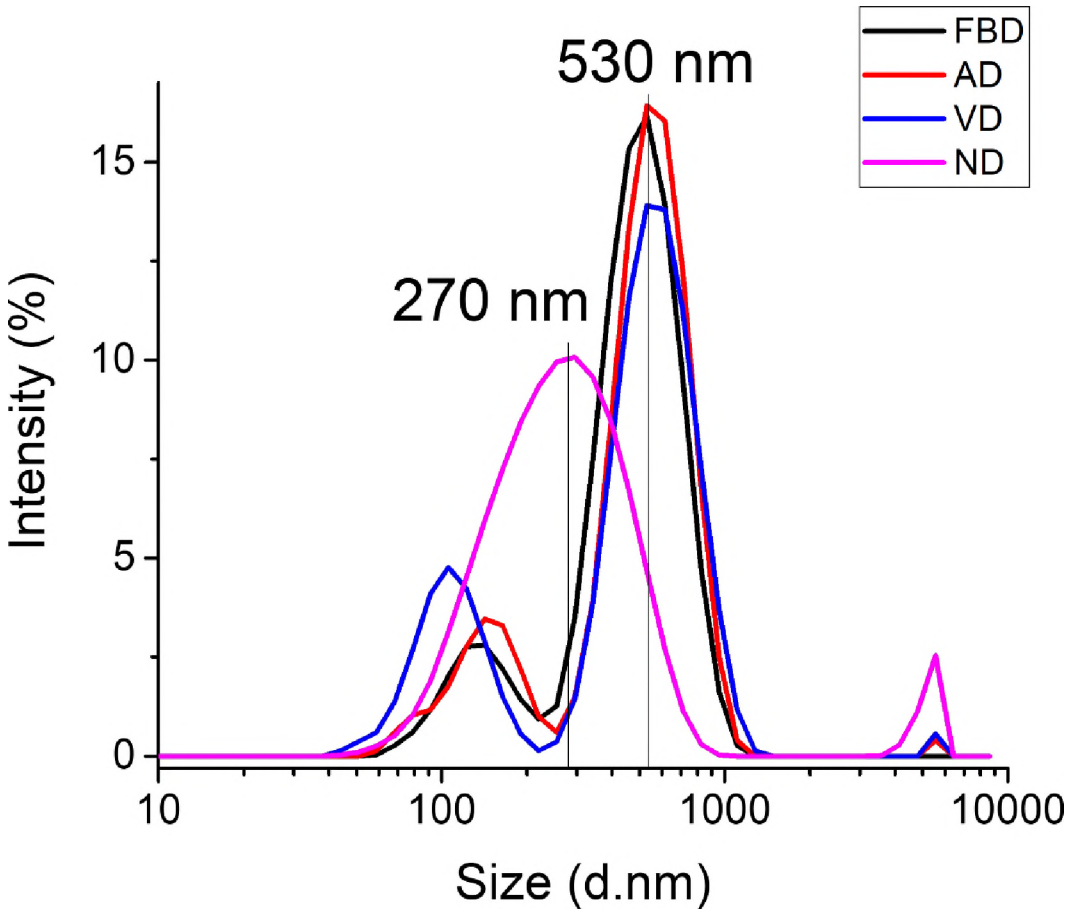

199

200 **Figure 3.** DLS profiles representing the particle size distribution of hydrated citrus fibers. Particles larger
201 than 8 μm were filtered out.
202

203 The ND suspension had one broad distribution of particle size centered at ~270 nm with a
204 polydispersity of 0.5. However, the FBD, AD, and VD suspensions showed bimodal distribution
205 bands – a small band at ~100 nm and a much large band at ~530 nm – with a polydispersity of 0.7.
206 This is clear evidence that fibers in the re-hydrated suspension were aggregated. In DLS, the shape
207 of aggregates is considered to be spherical, so the particle is not the real size of the fibrils[2]. In any
208 rate, the data suggest that the rehydration process cannot fully (re)disperse the fibers that were
209 aggregated during the drying process. This change in the particle size distribution may be the main
210 cause for the reduction of viscosity of the re-hydrated suspension compared to the ND suspension

211 (Figure 3). Because there was no noticeable difference in IR (sensitive to chemical bond length
212 scale) and XRD (sensitive to the crystal unit cell scale) for the dried samples (Figure 2), the main
213 cause responsible for different particle size distribution is likely the physical structures in the larger
214 length scale. For this reason, we used SFG to analyze the structural order or packing of citrus fibers
215 over the meso-scale which is determined by the coherence length of the SFG process.[11-13]
216
217 *Spectroscopic evidence for citrus peel fiber aggregation*

218 Classically, in SFG analysis of cellulose, the CH and OH stretch vibration regions are
219 analyzed[6, 8-9]. The CH stretch peaks are between 2800 cm^{-1} and 3000 cm^{-1}, and the OH stretch
220 peaks are between 3200 cm^{-1}-3600 cm^{-1}. Details of the peaks observed in these regions are
221 summarized in Table 1. In SFG analysis, the CH region is more sensitive to total concentration of
222 crystalline domains only, while the OH peaks are sensitive to both mesoscale arrangement and
223 concentration of the crystalline domains. Thus, the OH/CH intensity ratio could be used to study
224 mesoscale packing of cellulose microfibrils[12], the bundling of crystals[11], and the orientation of
225 fibers[10]. In addition, SFG can distinguish the OH functional groups exposed at the surface from
226 those in the bulk.[29] The phase mismatch between three waves (IR, 800 nm, and sum frequency) in
227 nonlinear process makes SFG well suited to characterize the mesoscale packing of cellulose
228 (>10nm to 100 nm).

229 SFG analysis was done for fibers in dried and hydrated conditions. As a nonlinear
230 spectroscopy technique, SFG is sensitive to both concentrations of SFG-active compounds and
231 their mesoscale oarganiztion. As evident by similar behavior of XRD diffractograms among
232 samples in Figure 2(b) , any change in the SFG spectrum must originate from variations in the
233 mesoscale packing of cellulose fibers. Figure 4(a) shows the SFG spectra of citrus fibers in the dry

state. For this experiment, the citrus fiber powder was made into a pellet, and the SFG analysis was done in reflection geometry.

Table 1. The peak assignment for CH and OH regions of cellulose SFG spectrum[9]. Reprinted from Makarem et al.[9], with permission from the Copyright Clearance Center. Copyright 2019, Springer Nature.

Frequency	Assignment
2850-2880 cm^{-1}	Symmetric bond stretching of CH_2
2944 cm^{-1},2968 cm^{-1}	Asymmetric bond stretching of CH_2
3240 cm^{-1}	intrachain OH Stretching at 2O–H···6O for cellulose Iα
3270 cm^{-1}	intrachain OH Stretching at 2O–H···6O for cellulose Iβ
3300-3330 cm^{-1}	OH Stretching of 2O–H···6O–H···3O–H···5O
3370 cm^{-1}	intrachain OH Stretching at 3O–H···5O
3410 cm^{-1}	intrachain OH Stretching at 6O–H···3O
3450 cm^{-1}	Stretching of surface OH groups with weak hydrogen bonding

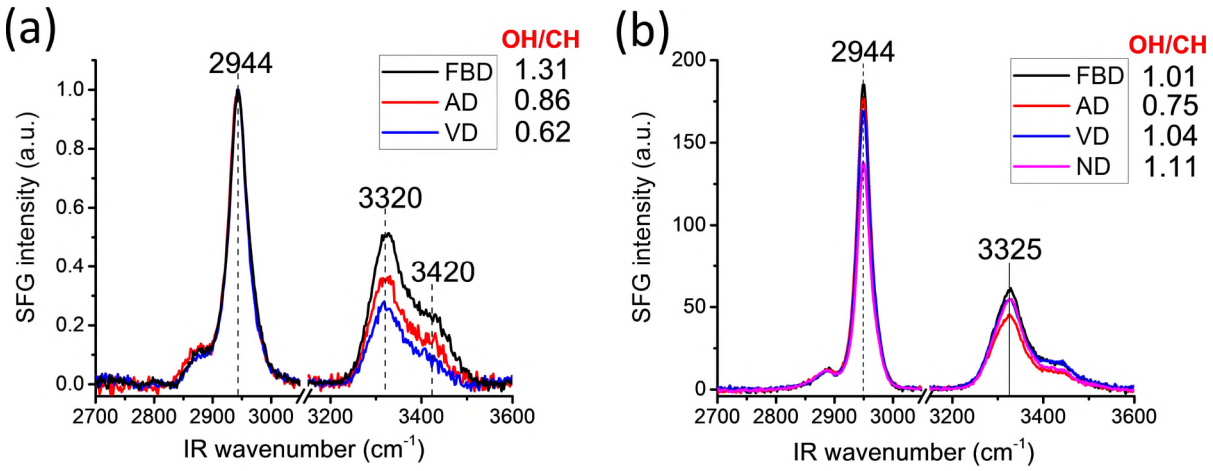

Figure 4. SFG spectra of citrus peel fibers in (a) the dehydrated state and (b) the suspension in D_2O. In (a), the 2944 cm^{-1} intensity was used as a reference for normalization; this was necessary because the absolute intensities of dried pellects could vary with the surface roughness of the sample. The ratio of OH and CH band areas is shown for each sample in (b).

Figure 4(a) represents the SFG spectra for FBD, AD, and VD in the dried state. First level SFG analysis includes assessing typical crystalline cellulose Iβ features– a strong and sharp peak at 2944 cm^{-1} assigned to the asymmetric stretch vibrations of the exocyclic CH_2 groups coupled with the axial CH groups and a broad peak at 3320 cm^{-1} peak assigned to the collective stretch vibrations of OH groups in the crystalline domain[29-30]. The shoulder peak at 3425 cm^{-1} can be attributed to weakly hydrogen-bonded OH groups that can be found at the surface of cellulose microfibrils[29, 31] as well as the OH groups in the physically strained region of cellulose microfibrils.[32] From the XRD analysis, we know that the citrus pectin can form the crystalline phase during the dehydration (see inset of Figure 2(b)); the crystalline form of isolated pectin can give a broad SFG features centered at ~2920 cm^{-1} and a shoulder peak at 2980 cm^{-1} with no peak at OH stretch region (see Figure S2). Comparing the SFG spectra of the isolated pectins and the citrus peel fibers, it can be concluded that pectins in the citrus fibers did not form SFG-active

260 crystalline forms. Their crystallization behavior may have been altered due to the presence of
261 cellulose and other components.[33-34]

262 The comparison of the SFG spectra of the FBD, VD, and AD fibers highlighted that the
263 OH/CH ratio was the largest for FBD sample and the smallest for AD sample. Previous studies
264 showed that the change in the OH/CH ratio of the cellulose SFG spectrum could be caused by the
265 change in inter-fibrillar distance. This was proved for unixaxially aligned cellulose microfibrils
266 without specific polarity.[12] In that case, the OH/CH ratio increases as the distance between
267 crystalline domains increases. The largest OH/CH ratio for the FBD could mean that non-cellulosic
268 compounds such as pectin were well dispersed between the cellulose microfibrils, making
269 cellulose fibrils more loosely packed, compared to the AD and VD processes. It seems like the VD
270 process produced most densely packed fibers, giving the lowest OH/CH intensity ratio. But, this
271 packing difference in the dry state did not seem to directly correlate with the viscosity of the re-
272 hydrated suspension (see Figure 1).

273 Figure 4(b) shows the SFG spectra of AD, VD, FBD, and ND suspensions in the hydrated
274 state (2%wt in D_2O). The SFG experiment of hydrated fibers was done in transmission geometry.
275 By using transmission geometry, the signal to noise ratio can be improved because of the much
276 longer SFG coherence length in transmission geometry (>10μm). It is noted that the 3420 cm^{-1}
277 component was much smaller in the rehydrated state than in the dry state. In D_2O, the surface OH
278 groups of crystalline cellulose were fully exchanged to the OD groups [29]; thus, they cannot
279 contribute to the SFG intensity in this condition. Then, the weak 3420 cm^{-1} component detected in
280 rehydrated state in D_2O must originate from weakly hydrogen-bonded OH groups due to physical
281 strains (kinks and bends or fibers) inside the crystalline domains to which D_2O didn't have access.

From Figure 4(b), it can be seen that the OH/CH ratio was the highest for the ND suspension. This high OH/CH ratio meant that the cellulose fibrils were well separated, which is consistent with the absence of aggregates in the DLS analysis for this sample (Figure 3). For the AD, VD, and FBD samples, the OH/CH intensity ratios in the rehydrated state (Figure 4b) were different from those in the dry state (Figure 4a). As an example, the OH/CH ratio for FBD in dry state was 1.31 and as it became hydrated it reduced to 1.01, on the contrary, the OH/CH ratio for VD in dry state was 0.62 and when hydrated it increased to 1.04. implying that the cellulose fibril packing in the dry state probed with SFG did not necessarily reflect the degree of dispersion after the rehydration.

In Figure 5, the viscosities and the OH/CH SFG ratios of the 2wt.% suspensions are plotted with respect to the average particle size determined from DLS. It can be seen that both viscosity and OH/CH SFG ratio decreased as the average particle size in the suspension increased. This result suggests that the viscosity of the citrus peel fiber solution was highly dependent on the degree of cellulose fibril aggregations. The quantitative relationship with the average particle size was different for the viscosity and the OH/CH SFG ratio because each characterization method measures different properties at different length scales.

The differences in the slopes observed at figure 5, can be rooted to the differences between the techniques used in this experiment. As previously mentioned, the SFG signal is sensitive to the concentration and packing of fibers.[8, 11] Because SFG is a nonlinear spectroscopy technique the changes in concentration or packing doesn't linearly correlate with the signal intensity. Also, the distance between fibers[12] and the way an individual microfibril is oriented with respect to its neighboring microfibrils can greatly affect the peak intensity and shape in both CH and OH stretch region. On the other hand, viscosity measurement is a macroscopic characterization technique and

it is independent of localized changes in orientation of microfibrils. Because of these inherent differences in these two techniques, although the OH/CH and viscosity measurements show similar trend their slopes are different, as observed in figure 5.

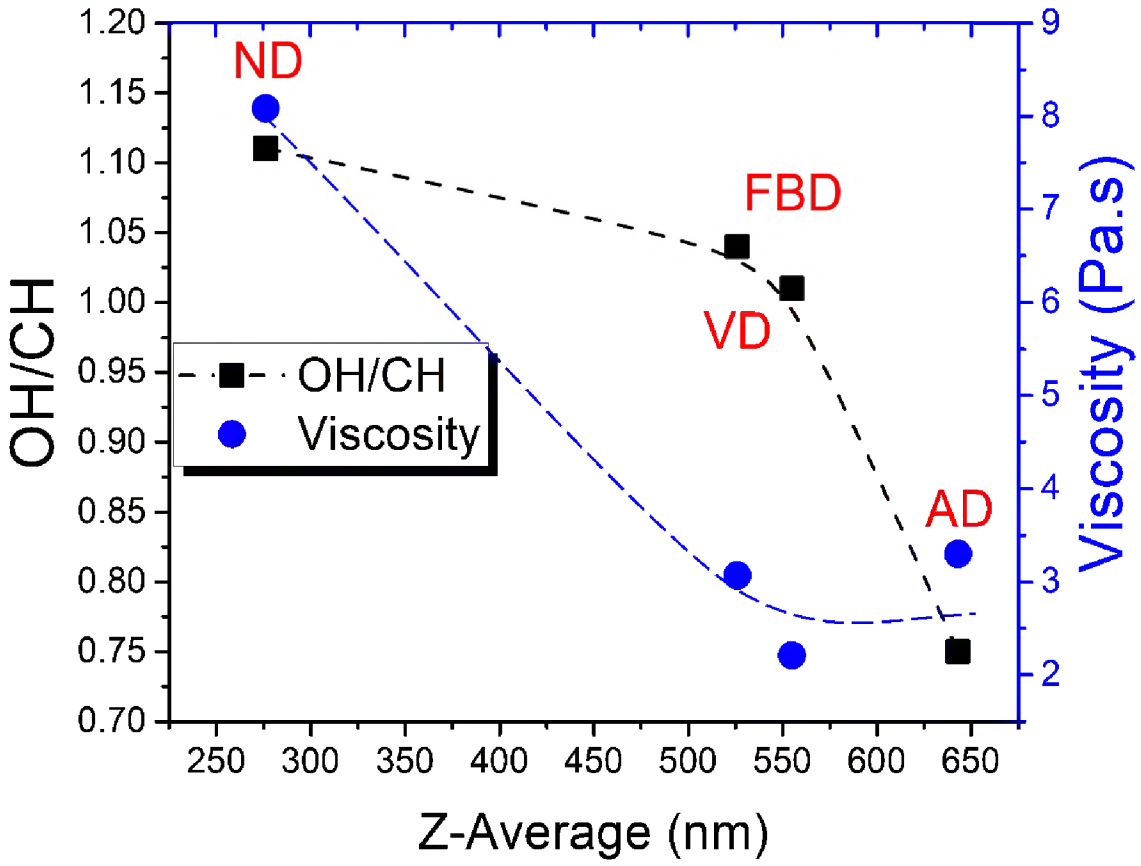

Figure 5. The correlation between average particle size, OH/CH ratio in SFG spectra, and viscosity at 10 1/s are illustrated here. The OH/CH ratio appears to decrease as the average particle size increases. The viscosity of fiber suspensions shows a monotonic decrease by increasing the average particle size. Both SFG and Viscosity show similar trend regarding the change in aggregates size.

Conclusion

This study investigated changes in nano- and meso-scale structures of citrus fiber fibers before (ND) and after drying in different conditions (AD, VD, and FBD). The ATR-IR and XRD showed no change in chemical composition or crystallinity in dehydrated fibers. By comparing the size distribution of rehydrated fibers (VD, AD, and FBD) with ND, it was found that there was a shift in size distribution toward larger particles in the suspensions of dehydrated fibers. Comparing SFG spectra of ND and rehydrated fibers indicated that the packing of fibers was seperated more greatly when they were initially hydrated, while the packing of re-hydrated fibers became denser. This study found that the viscosity of fiber suspension correlated with the mesoscale aggregation of fibers and particle size distribution. Since the factors which govern the irreversible aggregation of fibers could not be determined in this study, further studies are needed to better understand the key parameters controlling the redispersion of citrus fibers.

Acknowledgment

This contribution was identified by Dr. Hugh O'Neill (Oak Ridge National Labratory) as the Best Presentation in the "Interplay of Cellulose & Other Biopolymers in Biological & Designed Materials Systems" session of the 2019 ACS Spring National Meeting in Orlando. This study was supported by Cargill Inc. The SFG system used in this study was constructed with the support of Center for Lignocellulose Structure and Formation, an Energy Frontier Research Center funded by Department of Energy, Office of Science, Basic Energy Sciences under Award # DE-SC0001090.

Supporting information

Figure S1; viscosity versus shear rate for citrus fiber suspensions prepared in two different fluidized-bed drying condition. Figure S2; the IR spectra of pectin in different degrees of demethylsterification.

References

1. Wallecan, J.; McCrae, C.; Debon, S. J. J.; Dong, J.; Mazoyer, J., Emulsifying and Stabilizing Properties of Functionalized Orange Pulp Fibers. *Food Hydrocolloids* **2015**, *47*, 115-123.
2. Willemsen, K. L. D. D.; Panozzo, A.; Moelants, K.; Debon, S. J. J.; Desmet, C.; Cardinaels, R.; Moldenaers, P.; Wallecan, J.; Hendrickx, M. E. G., Physico-Chemical and Viscoelastic Properties of High Pressure Homogenized Lemon Peel Fiber Fraction Suspensions Obtained after Sequential Pectin Extraction. *Food Hydrocolloids* **2017**, *72*, 358-371.
3. Kwak, H. W.; You, J.; Lee, M. E.; Jin, H.-J., Prevention of Cellulose Nanofibril Agglomeration During Dehydration and Enhancement of Redispersibility by Hydrophilic Gelatin. *Cellulose* **2019**, *26*, 4357-4369.
4. Peng, Y.; Gardner, D. J.; Han, Y., Drying Cellulose Nanofibrils: In Search of a Suitable Method. *Cellulose* **2012**, *19*, 91-102.
5. Lambert, A. G.; Davies, P. B.; Neivandt, D. J., Implementing the Theory of Sum Frequency Generation Vibrational Spectroscopy: A Tutorial Review. *Appl. Spectrosc. Rev.* **2005**, *40*, 103-145.
6. Barnette, A. L.; Bradley, L. C.; Veres, B. D.; Schreiner, E. P.; Park, Y. B.; Park, J.; Park, S.; Kim, S. H., Selective Detection of Crystalline Cellulose in Plant Cell Walls with Sum-Frequency-Generation (Sfg) Vibration Spectroscopy. *Biomacromolecules* **2011**, *12*, 2434-9.
7. Lee, C. M.; Mittal, A.; Barnette, A. L.; Kafle, K.; Park, Y. B.; Shin, H.; Johnson, D. K.; Park, S.; Kim, S. H., Cellulose Polymorphism Study with Sum-Frequency-Generation (Sfg) Vibration Spectroscopy: Identification of Exocyclic Ch2oh Conformation and Chain Orientation. *Cellulose* **2013**, *20*, 991-1000.
8. Barnette, A. L.; Lee, C.; Bradley, L. C.; Schreiner, E. P.; Park, Y. B.; Shin, H.; Cosgrove, D. J.; Park, S.; Kim, S. H., Quantification of Crystalline Cellulose in Lignocellulosic Biomass Using Sum Frequency Generation (Sfg) Vibration Spectroscopy and Comparison with Other Analytical Methods. *Carbohydr Polym* **2012**, *89*, 802-9.
9. Makarem, M.; Lee, C. M.; Kafle, K.; Huang, S.; Chae, I.; Yang, H.; Kubicki, J. D.; Kim, S. H., Probing Cellulose Structures with Vibrational Spectroscopy. *Cellulose* **2019**, *26*, 35-79.
10. Chen, X.; Lee, C. M.; Wang, H.-F.; Jensen, L.; Kim, S. H., Experimental and Theoretical Study of Azimuth Angle and Polarization Dependences of Sum-Frequency-Generation Vibrational Spectral Features of Uniaxially Aligned Cellulose Crystals. *J. Phys. Chem. C* **2017**, *121*, 18876-18886.
11. Lee, C. M.; Kafle, K.; Park, Y. B.; Kim, S. H., Probing Crystal Structure and Mesoscale Assembly of Cellulose Microfibrils in Plant Cell Walls, Tunicate Tests, and Bacterial Films Using Vibrational Sum Frequency Generation (Sfg) Spectroscopy. *Phys Chem Chem Phys* **2014**, *16*, 10844-53.
12. Makarem, M.; Sawada, D.; O'Neill, H. M.; Lee, C. M.; Kafle, K.; Park, Y. B.; Mittal, A.; Kim, S. H., Dependence of Sum Frequency Generation (Sfg) Spectral Features on the Mesoscale Arrangement of Sfg-Active Crystalline Domains Interspersed in Sfg-Inactive Matrix: A Case Study with Cellulose in Uniaxially Aligned Control Samples and Alkali-Treated Secondary Cell Walls of Plants. *J. Phys. Chem. C* **2017**, *121*, 10249-10257.
13. Lee, C. M.; Chen, X.; Weiss, P. A.; Jensen, L.; Kim, S. H., Quantum Mechanical Calculations of Vibrational Sum-Frequency-Generation (Sfg) Spectra of Cellulose: Dependence of the Ch and Oh Peak Intensity on the Polarity of Cellulose Chains within the Sfg Coherence Domain. *J. Phys. Chem. Lett.* **2017**, *8*, 55-60.

14. Stetefeld, J.; McKenna, S. A.; Patel, T. R., Dynamic Light Scattering: A Practical Guide and Applications in Biomedical Sciences. *Biophys. Rev.* **2016**, *8*, 409-427.
15. Kacurakova, M.; Capek, P.; Sasinkova, V.; Wellner, N.; Ebringerova, A., Ft-Ir Study of Plant Cell Wall Model Compounds: Pectic Polysaccharides and Hemicelluloses. *Carbohydr. polym.* **2000**, *43*, 195-203.
16. Kafle, K.; Park, Y. B.; Lee, C. M.; Stapleton, J. J.; Kiemle, S. N.; Cosgrove, D. J.; Kim, S. H., Effects of Mechanical Stretching on Average Orientation of Cellulose and Pectin in Onion Epidermis Cell Wall: A Polarized Ft-Ir Study. *Cellulose* **2017**, *24*, 3145-3154.
17. Wilson, R. H.; Smith, A. C.; Kačuráková, M.; Saunders, P. K.; Wellner, N.; Waldron, K. W., The Mechanical Properties and Molecular Dynamics of Plant Cell Wall Polysaccharides Studied by Fourier-Transform Infrared Spectroscopy. *Plant physiol.* **2000**, *124*, 397.
18. Xu, F.; Yu, J.; Tesso, T.; Dowell, F.; Wang, D., Qualitative and Quantitative Analysis of Lignocellulosic Biomass Using Infrared Techniques: A Mini-Review. *Appl. Energy* **2013**, *104*, 801-809.
19. Kim, H. J.; Lee, C. M.; Dazen, K.; Delhom, C. D.; Liu, Y.; Rodgers, J. E.; French, A. D.; Kim, S. H., Comparative Physical and Chemical Analyses of Cotton Fibers from Two near Isogenic Upland Lines Differing in Fiber Wall Thickness. *Cellulose* **2017**, *24*, 2385-2401.
20. Abidi, N.; Hequet, E.; Cabrales, L.; Gannaway, J.; Wilkins, T.; Wells, L. W., Evaluating Cell Wall Structure and Composition of Developing Cotton Fibers Using Fourier Transform Infrared Spectroscopy and Thermogravimetric Analysis. *J. Appl. Polym. Sci.* **2008**, *107*, 476-486.
21. Liu, Y., Recent Progress in Fourier Transform Infrared (Ftir) Spectroscopy Study of Compositional, Structural and Physical Attributes of Developmental Cotton Fibers. *Materials* **2013**, *6*, 299-313.
22. Sene, C. F.; McCann, M. C.; Wilson, R. H.; Grinter, R., Fourier-Transform Raman and Fourier-Transform Infrared Spectroscopy (an Investigation of Five Higher Plant Cell Walls and Their Components). *Plant physiol.* **1994**, *106*, 1623-1631.
23. Synytsya, A.; Čopíková, J.; Matějka, P.; Machovič, V., Fourier Transform Raman and Infrared Spectroscopy of Pectins. *Carbohydr. polym.* **2003**, *54*, 97-106.
24. Park, S.; Baker, J. O.; Himmel, M. E.; Parilla, P. A.; Johnson, D. K., Cellulose Crystallinity Index: Measurement Techniques and Their Impact on Interpreting Cellulase Performance. *Biotechnol. Biofuels* **2010**, *3*, 10.
25. Lee, C.; Dazen, K.; Kafle, K.; Moore, A.; Johnson, D. K.; Park, S.; Kim, S. H., Correlations of Apparent Cellulose Crystallinity Determined by Xrd, Nmr, Ir, Raman, and Sfg Methods. In *Cellulose Chemistry and Properties: Fibers, Nanocelluloses and Advanced Materials*, Rojas, O. J., Ed. Springer International Publishing: Cham, 2016; pp 115-131.
26. Girija, E. K.; Charistic Latha, S.; Narayama Kalkura, S.; Subramanian, C.; Ramasamy, P., Crystallization and Microhardness of Calcium Oxalate Monohydrate. *Materials Chemistry and Physics* **1998**, *52*, 253-257.
27. Luckham, P. F.; Ukeje, M. A., Effect of Particle Size Distribution on the Rheology of Dispersed Systems. *Journal of Colloid and Interface Science* **1999**, *220*, 347-356.
28. Genovese, D. B., Shear Rheology of Hard-Sphere, Dispersed, and Aggregated Suspensions, and Filler-Matrix Composites. *Adv. Colloid Interface Sci.* **2012**, *171-172*, 1-16.
29. Makarem, M.; Lee, C. M.; Sawada, D.; O'Neill, H. M.; Kim, S. H., Distinguishing Surface Versus Bulk Hydroxyl Groups of Cellulose Nanocrystals Using Vibrational Sum Frequency Generation Spectroscopy. *J. Phys. Chem. Lett.* **2018**, *9*, 70-75.
30. Ling, Z., et al., Effects of Ball Milling on the Structure of Cotton Cellulose. *Cellulose* **2019**, *26*, 305-328.
31. Olsson, A.-M.; Salmén, L., The Association of Water to Cellulose and Hemicellulose in Paper Examined by Ftir Spectroscopy. *Carbohydr. Res.* **2004**, *339*, 813-818.

32. Huang, S.; Makarem, M.; Kiemle, S. N.; Zheng, Y.; He, X.; Ye, D.; Gomez, E. W.; Gomez, E. D.; Cosgrove, D. J.; Kim, S. H., Dehydration-Induced Physical Strains of Cellulose Microfibrils in Plant Cell Walls. *Carbohydr. polym.* **2018**, *197*, 337-348.
33. Rim, P. B.; Runt, J. P., Melting Behavior of Crystalline/Compatible Polymer Blends: Poly (Iε-Caprolactone)/Poly (Styrene-Co-Acrylonitrile). *Macromolecules* **1983**, *16*, 762-768.
34. Rabiej, S.; Kwiatkowski, R.; Wlochowicz, A., *Determination of the Crystallinity of Polymer Blends*; SPIE, 1997; Vol. 3095.